Recombination Time Mismatch and Spin Dependent Photocurrent at a Ferromagnetic-Metal–Semiconductor Tunnel Junction

Viatcheslav I. Safarov,[1] Igor V. Rozhansky,[1,2] Ziqi Zhou,[3,4] Bo Xu,[5] Zhongming Wei,[4] Zhan-Guo Wang,[6,7] Yuan Lu,[3] Henri Jaffrès,[8] and Henri-Jean Drouhin[1,*]

[1]*LSI, École Polytechnique, CEA/DRF/IRAMIS, CNRS, Institut Polytechnique de Paris, 91128 Palaiseau, France*
[2]*Ioffe Institute, St. Petersburg 194021, Russia*
[3]*Institut Jean Lamour, Université de Lorraine, CNRS UMR7198, Campus ARTEM, 2, allée André Guinier, BP 50840, 54011 Nancy, France*
[4]*State Key Laboratory of Superlattices and Microstructures, Institute of Semiconductors, Chinese Academy of Sciences and Center of Materials Science and Optoelectronics Engineering, University of Chinese Academy of Sciences, Beijing 100083, China*
[5]*Key Laboratory of Semiconductor Materials Science, Institute of Semiconductors, Chinese Academy of Sciences, P. O. Box 912, Beijing 100083, China*
[6]*Institute of Semiconductors, Chinese Academy of Sciences, Beijing 100083, China*
[7]*Center of Materials Science and Optoelectronics Engineering, University of Chinese Academy of Sciences, Beijing 100049, China*
[8]*Unité Mixte de Physique, CNRS, Thales, Université Paris Saclay, 91767 Palaiseau, France*

(Received 5 August 2021; accepted 14 December 2021; published 3 February 2022)

We report on carrier dynamics in a spin photodiode based on a ferromagnetic-metal–GaAs tunnel junction. We show that the helicity-dependent current is determined not only by the electron spin polarization and spin asymmetry of the tunneling but in great part by a dynamical factor resulting from the competition between tunneling and recombination in the semiconductor, as well as by a specific quantity: the charge polarization of the photocurrent. The two latter factors can be efficiently controlled through an electrical bias. Under longitudinal magnetic field, we observe a strong increase of the signal arising from inverted Hanle effect, which is a fingerprint of its spin origin. Our approach represents a radical shift in the physical description of this family of emerging spin devices.

DOI: 10.1103/PhysRevLett.128.057701

Spin optoelectronics, which uses the ability to interconvert a photon spin to a charge or vice versa, covers a broad range of disruptive interdisciplinary applications. It has the potential to revolutionize telecommunications, opening up a new avenue for reaching THz modulation frequencies [1]. Circularly polarized light also enables transmission of the spin information, thus providing a solution to the problem of interconnection of spintronic devices. Important efforts were devoted to the conception of circularly polarized light emitters, decisive achievements being the spin light emitting diodes [2–5] and the introduction of the spin-laser concept by Žutić *et al.* [6] and Lindemann *et al.* [7], now implemented in spin vertical-cavity surface-emitting lasers. Reciprocal devices are solid-state helicity detectors converting the helicity of the light into spin polarization of photogenerated electrons. An electrical signal is detected thanks to spin dependent photocurrent, resulting from transport phenomena in all-semiconductor devices [8,9] or tunneling into a ferromagnetic (FM) contact. However, the realization of efficient spin photodiodes has remained a challenge for more than two decades [1,8–21] and the underlying physics is far from being clearly understood. While a variety of materials and structures have the ability to produce helicity-dependent signals, potential devices are based on the combination of well-mastered materials and technologically mature heterostructures suited for room temperature operation [1], e.g., GaAs-like direct band-gap semiconductors where spin-polarized electrons can be generated by optical orientation [22], MgO active insulators, which are the building blocks of hard-drive read heads and magnetic random access memories, and FM contacts, whereas, in parallel, new routes are being explored, e.g., using hybrid organic-inorganic materials [23–25].

Up to now, optical spin injection in spin photodiodes was analyzed by analogy to spin dependent tunneling in FM tunnel junctions, which involves only the electron spin polarization and spin asymmetry of the tunneling. Here, we reveal that the spin signal is largely determined by a dynamical factor arising from the competition between tunneling into the ferromagnet and recombination with the holes. This recombination time mismatch is fundamental as it can strongly reduce the spin asymmetry in close analogy with the famous impedance-mismatch problem for electrical spin injection [21,26].

Spin-related effects are classically identified from the polarization decrease under the application of an external magnetic field perpendicular to the spin direction (normal Hanle effect [22]). In our experimental geometry where the

FM layer magnetization is normal to the surface (perpendicular magnetic anisotropy, or PMA), this is not straightforward because the *in-plane* component of the external field would affect not only the electron spin but also the magnetization direction. Having introduced quantum dots (QDs) in the active region of the spin photodiode, we observe a large *inverted* Hanle effect, which results in an increase in polarization under the application of a magnetic field along the spin and magnetization direction. Thus, the *perpendicular* magnetic field does not affect the magnetization and constitutes a specific probe of the electron spin contribution [27].

The spin photodiode consists of a FM/MgO/semiconductor structure initially optimized for the realization of spin light emitting diodes; similar structures were extensively described in Refs. [4,5,21,28], where details concerning the growth and characterization can be found. The stack includes a heavily p-doped GaAs substrate, a AlGaAs barrier, an i-GaAs layer with delta p-doping containing InGaAs QDs, and an n-GaAs layer topped with a MgO tunnel barrier and a CoFeB FM layer capped with Ta; a full description is given in the Supplemental Material (SM) [29].

The coercive field was found to be about 10 mT with a 100% remanence at liquid-nitrogen temperature. Then 300 μm diameter circular mesas were processed and the PMA of the FM layer was established by rapid thermal annealing.

The sample is illuminated perpendicularly to the surface by a low-noise 785-nm laser diode. The light helicity is modulated from right (σ^+) to left (σ^-) handed at 50 kHz through a photoelastic modulator and the ac component of the photocurrent i_{ac} is detected by a lock-in amplifier. The bias voltage is applied to the semiconductor substrate while keeping the front ferromagnetic contact grounded. All the measurements are performed at liquid-nitrogen temperature.

Figure 1 presents the band diagram of the diode for different biases V_b and dc $I(V_b)$ characteristics in the dark and under illumination for three different light powers in the ratio 1.0/0.6/0.2. Under strong reverse bias ($V_b = -0.4$ V), the photocurrent I_p is proportional to the light power impinging on the device. The $I(V_b)$ characteristics at forward bias are typical for tunnel junctions (inset). At $V_b \simeq 0.75$ V, the photocurrent I_p cancels and changes its sign beyond this compensation point, indicating that the photocurrent I_p consists of two components (defined here as positive quantities), one originating from photogenerated electrons (I_{pe}) and the other due to photogenerated holes (I_{ph}), with the relation $I_p = I_{\mathrm{pe}} - I_{\mathrm{ph}}$.

Under σ^+ (σ^-) excitation, electrons are promoted into the conduction band of GaAs with an initial spin polarization $P^* = -0.5$ ($+0.5$) [22,30] whereas, due to the extremely fast relaxation of their spins, the holes are unpolarized so that i_{ac} is related to the electron spin asymmetry. The asymmetry of the spin dependent tunneling can be characterized by the tunneling times $\tau_\pm = \tau_t \mp \Delta\tau_t$, where the $\pm$ signs refer to parallel or antiparallel orientations of the magnetization and incoming electron spins. The tunneling asymmetry $\mathcal{A}_s$ is defined as $\mathcal{A}_s = \Delta\tau_t/\tau_t$. We also account for the intensity modulation originating from the polarization-dependent magnetic circular dichroism (MCD) when the laser beam crosses the FM layer; the corresponding coefficient δ changes its sign upon magnetization reversal like $\mathcal{A}_s$ does. Note that δ acts both on the electron and hole currents whereas $\mathcal{A}_s$ only affects the electron current.

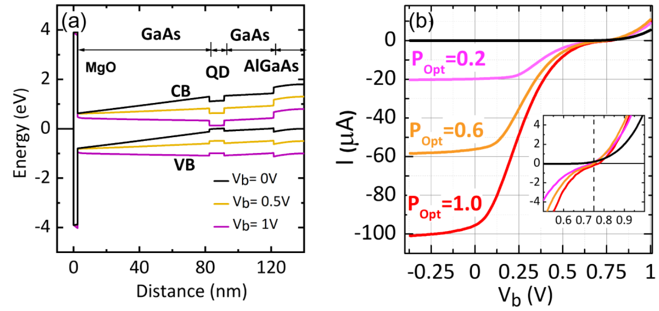

FIG. 1. (a) Band profile of the semiconductor stack for different electrical bias (V_b) applied to the substrate, the FM metal top layer being grounded. (b) $I(V)$ curves in the dark (black) and under light excitation with powers in the ratio 1.0/0.6/0.2. Inset: Enlargement of the high-impedance forward domain around $V_b = 0.75$ V.

Starting from the spin and charge conservation equations, it can be shown (SM) that

$$\begin{aligned} i_{\mathrm{ac}} &= P_s \mathcal{A}_s I_{\mathrm{pe}} + \delta(I_{\mathrm{pe}} - I_{\mathrm{ph}}) \\ P_s &= P^* \frac{1}{1 + \frac{\tau_r}{T_1} + \frac{\tau_r}{\tau_t}}, \end{aligned} \tag{1}$$

where τ_r is the electron recombination time inside the semiconductor active region and T_1 is the longitudinal spin relaxation time. Note that the effective polarization P_s is not simply the equilibrium spin polarization in the semiconductor under optical pumping as it contains the important dynamical factor τ_r/τ_t; P_s vanishes at $\tau_r \to \infty$ or $\tau_t \to 0$ when all the photogenerated electrons are extracted from the semiconductor regardless of their spin orientation. We emphasize that (at a given spin relaxation time) the spin dependent current is scaled by the competition between recombination and tunneling. The optimum is reached (Eqs. (S11) and (S12) of the SM) when the two times are matched according to $\tau_t = \tau_r\sqrt{T_1/(T_1 + \tau_r)}$. This is analogous to the impedance mismatch problem as mentioned in Ref. [21].

Under negative (reverse) bias, the total photocurrent $I_p = I_{\mathrm{pe}}$ is an electron photocurrent and, because no holes are available for recombination near the tunnel barrier (electrons and holes are separated by the electric field), $\tau_r \gg \tau_t$ so that P_s vanishes: i_{ac} is related to the MCD rather

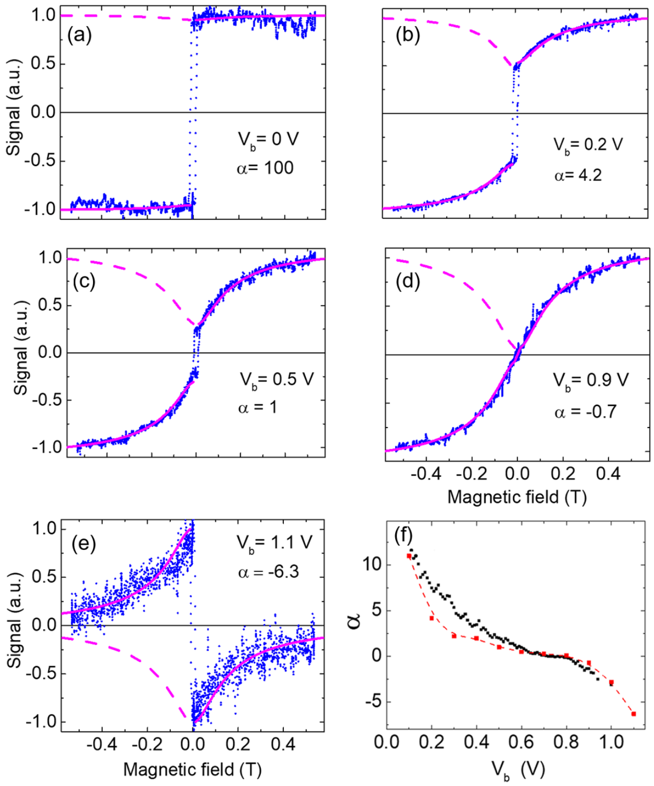

FIG. 2. Polarization-dependent photocurrent i_{ac} versus longitudinal magnetic field B for several V_b (a)–(e). Blue dots: Experimental data; magenta full lines: fits—the relevant V_b and α are indicated and dashed lines are added to illustrate the inverted Hanle effect. Figure 2(f) (red circles) shows the variation of α with V_b extracted from the fits (a)–(e) and at other values of V_b not presented here. The black dotted curve shows the variation of the fitting parameter α extracted from normalized signal measurements.

than to the electron spin polarization so that there is no effect of the external magnetic field beyond the hysteresis loop, as shown in Fig. 2(a) measured at $V_b = 0$ V. The measurement of the asymmetry i_{ac}/I_p is a direct determination of δ yielding $\delta = 0.24\%$. Note the hysteresis cycles in Figs. 2(a)–(c) and (e). Under positive (forward) bias, a striking observation is the increase of the signal with increasing $B = |\mathbf{B}|$ after magnetization reversal [Figs. 2(b)–(d)]. The magnetization being saturated, this increase can only be attributed to an increase of P_s and thus constitutes an unambiguous signature of a spin effect.

The preceding conclusions are further supported by measurements performed under oblique field, for **B** lying at 65.5° and 78° with respect to the normal to the surface (Fig. 3), the signal being proportional to the projection of the spin on the magnetization direction. At $V_b = 0$ V the variation of i_{ac} with B merely reflects the magnetization rotation whereas, for large positive biases, the change of P_s strongly affects the shape of the curves.

For structures with an in-plane magnetization, an increase of the electron spin polarization under an external magnetic

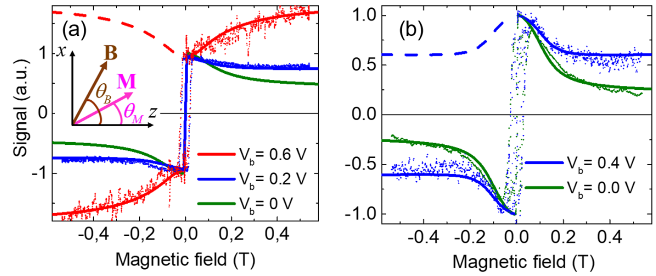

FIG. 3. Polarization-dependent photocurrent i_{ac} under oblique magnetic field for several values of V_b: (a) $\theta_B = 78°$; (b) $\theta_B = 65°$. Dotted lines: Experimental data. Solid lines: Fits using the same parameters as in Fig. 2. Inset: Orientation of the magnetization **M** and external magnetic field **B**; the z axis corresponds to the normal to the interface.

field parallel to the electron spin was reported [27,31]. This phenomenon was named the "inverted Hanle effect" in contrast to the regular Hanle effect and attributed to the compensation of static random stray fields produced near the FM layer due to the interface roughness. However, in our case with PMA, the stray fields are known to be much weaker than in the in-plane geometry [5,32,33] and cannot explain the observed large variation of the signal with the magnetic field on the scale of ~0.1 T. Also note that, for isotropic stray fields, the polarization enhancement would be limited to a factor of 3 [Ref. [27], Eq. (A-14)], which would be by far too small to account for our experimental data.

Then, we describe spin relaxation as the result of electron-spin interaction with random magnetic fields fluctuating in time with a correlation time τ_c analogously to the motional narrowing of NMR lines. The spin relaxation is suppressed by an external magnetic field: [30]

$$T_1 = \tau_{s0}(1 + \Omega^2\tau_c^2), \tag{2}$$

where T_1 is the longitudinal spin relaxation time, τ_{s0} is the spin relaxation time in the absence of external magnetic field, $\Omega = g^*\mu_B B/\hbar$ is the Larmor frequency, μ_B being the Bohr magneton, and g^* the Landé factor. As can be seen from Eq. (1), the magnetic field dependence in Eq. (2) leads to the increase of the signal when increasing B. Similar effects were reported in early pure-optical experiments on p-type AlGaAs [34]. Regarding the origin of the fluctuating magnetic fields, it is known that spin relaxation due to hyperfine interaction with unpolarized nuclei is very weak [34–36]. We focus on electron-hole exchange interaction and, in this case, the correlation time is the time spent by an electron in a localized state before being detrapped: the QDs located in the i layer close to the interface may provide such shallow traps, active for both photoelectrons and holes, giving them the opportunity to interact on the same sites. All the fits discussed hereafter use the value $g^* = -0.44$ (GaAs); the shape of the variation of i_{ac} versus B is not determined by a unique value of τ_c but by a quite broad distribution of correlation times, taken as a normal distribution with the average $\tau_{c0} = 390$ ps and dispersion $\sigma_{\tau_c} = 0.7\tau_{c0}$. These correlation times are much longer than the typical scattering time for conduction electrons, in the ps range, consistent with localized electrons.

For a convenient description of the helicity-dependent current on the electrical bias, we introduce a new parameter: the charge polarization of the photocurrent $\Pi = -(I_{\rm pe} - I_{\rm ph})/(I_{\rm pe} + I_{\rm ph})$. Π takes the value -1 when the photocurrent is a pure electron current and $\Pi = 0$ at the compensation point. The $I(V)$ characteristics closely reflect the Π variation. Then Eq. (1) can be rewritten as

$$i_{\rm ac} = I_p\left(\frac{\Pi - 1}{2\Pi} P_s \mathcal{A}_s + \delta\right) \tag{3}$$

It is convenient to introduce the ratio α between the MCD and optical-orientation induced terms of $i_{\rm ac}$ at $B = 0$ (reflected by $P_s(0)$):

$$\alpha = \frac{\delta(I_{\rm pe} - I_{\rm ph})}{P_s(0)\mathcal{A}_s I_{\rm pe}} = \frac{2\Pi}{\Pi - 1}\frac{\delta}{P_s(0)\mathcal{A}_s}. \tag{4}$$

From Eqs. (1) and (4), the dependence of the signal on B is given by

$$i_{\rm ac} \propto \frac{\alpha}{1 + \tau/\tau_{s0}} + \frac{1 + \Omega^2\tau_c^2}{1 + \Omega^2\tau_c^2 + \tau/\tau_{s0}}, \tag{5}$$

where the total electron lifetime is $\tau^{-1} = \tau_r^{-1} + \tau_t^{-1}$. Eq. (5) has been used to fit the curves obtained at different V_b (Fig. 2). For all the fits, the only bias-dependent parameter α is indicated in the plots [Figs. 2(a)–(e)]; Figure 2(f) shows the dependence of α on V_b. The consistency of all the fits requires $\tau/\tau_{s0} = 5.5$ independently of bias. This requirement can be satisfied provided $\tau_r/\tau_t \gg 1$ whatever the bias. Observe the evolution of the hysteresis cycle in Figs. 2(a)–(e): its relative amplitude diminishes with increase of the forward bias due to the decrease of the MCD contribution to the signal according to Eq. (1) which vanishes at the compensation point $I_{\rm pe} = I_{\rm ph}$; at a larger bias, the hole current becomes predominant ($\Pi > 0$) leading to the sign reversal of the MCD contribution, thus emphasizing the key role of the hole current.

The same set of parameters was used to fit the data obtained under oblique magnetic field. Now θ_B and θ_M are the angles between the normal to the surface **z** and **B**, **M**, respectively; θ_M is obtained by minimization of the total magnetic energy, involving the effective surface anisotropy term and the Zeeman interaction (Fig. 3(a), inset). One obtains (SM)

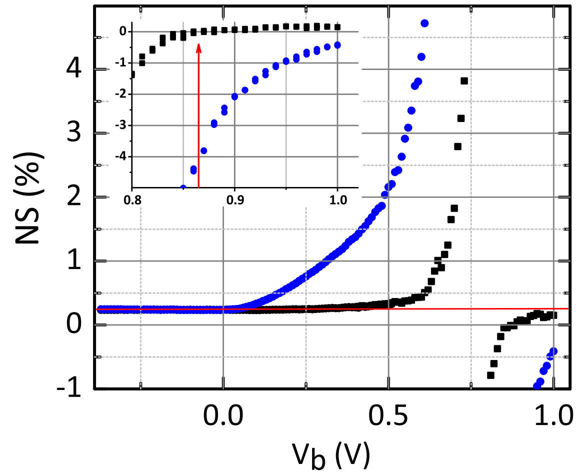

FIG. 4. Normalized magnetic signal (NS) versus V_b for the magnetic field $B = 0$ (black squares) and $B = 0.5$ T (blue circles). Inset: Enlargement of the high-forward-bias domain, showing the point where the hysteresis loop vanishes (arrow).

$$\begin{aligned} i_{\rm ac} \propto \cos\theta_M\left(1 + \frac{\alpha}{1 + \tau/\tau_{s0}}\right) \\ - \frac{\tau/\tau_{s0}}{1 + \Omega^2{\tau_c}^2 + \tau/\tau_{s0}}\cos\theta_B\cos(\theta_B - \theta_M) \\ - \sin\theta_B\sin(\theta_B - \theta_M)\frac{\tau/\tau_{s0}}{1 + \tau/\tau_{s0}}. \end{aligned} \tag{6}$$

As Eq. (6) suggests, the dependence of the electron spin projection on the magnetization contains competing contributions. First, the variation of the magnetization angle θ_M leads to the decrease of the spin projection on the magnetization direction with increase of B. Second, the suppression of the spin relaxation reflected by the middle term in Eq. (6) leads to an amplification of the signal asymmetry with B due to the inverted Hanle effect. The net result depends on the magnetic field orientation and magnitude. Figure 3 shows that the experimental data are well fitted with Eq. (6), using the same parameters as in Fig. 2.

To obtain a quantitative estimation of the helicity asymmetry, we need to know the total photocurrent I_p. However, due to the electrical characteristics of the circuit, a dc measurement of I_p would not be adequate: it is suitable to measure it under conditions identical to those under which we measure $i_{\rm ac}$. Therefore, we generate a small sine modulation of the laser-diode intensity at a frequency close to the operation frequency of the photoelastic modulator and determine I_p from the lock-in output signal. This signal was used to normalize the spin signal by the total photocurrent. The normalized signal (NS) is presented in Fig. 4. We observe that NS increases with bias starting from the value $\delta = 0.24\%$ at $V_b = -0.4$ V, completely determined by the MCD as already discussed [37], to reach 5% for $V_b = 0.6$ V under large B.

At the compensation point, the term proportional to δ in i_{ac} and, hence, α vanishes: in the series of data shown in Fig. 4, this occurs at $V_B = 0.75$ V and, in a domain of a few hundredth mV around it ($0.5\ \mathrm{V} \leq V_b \leq 0.8\ \mathrm{V}$), we observe that $I_{pe} \simeq I_{ph}$ so that i_{ac} is a *pure spin signal*, any contribution of the MCD being eliminated. This is a domain where the device is operated in the photovoltaic mode and where photodiodes have a high sensitivity. According to Eq. (1), NS can be written as

$$\mathrm{NS} = \delta - \frac{1-\Pi}{2\Pi} P_s \mathcal{A}_s. \tag{7}$$

At large forward bias, NS converges toward δ when the hole current becomes dominant—the smaller P_s, the faster the convergence. Obviously, NS diverges at the compensation point where $I_p = 0$. For a given B, there exists a point where i_{ac} vanishes. Considering such a point for $B = 0$, it is straightforward to check that NS measured for a higher B value expresses as $\mathrm{NS} = \delta[1 - P_s(B)/P_s(0)]$. From $\mathrm{NS} = -4.5\%$ at $B = 0.5$ T in Fig. 4, with $\delta = 0.24\%$, we directly find $P_s(B)/P_s(0) = 19$. As follows from Eqs. (4) and (7), α can be directly extracted from NS at zero magnetic field (Fig. 4, black squares): $\alpha = \delta(\mathrm{NS} - \delta)^{-1}$. The result shown in Fig. 2(f)—black dotted curve—is in fairly good agreement with the red points showing the values of α providing the best fit for the magnetic field dependence of the signal (in the experimental determination of α from NS, the error $\Delta\alpha \propto \alpha^2\Delta(\mathrm{NS})$ is large for large α).

In the present study, we unambiguously isolate the spin contribution to the helicity-dependent photocurrent from its dramatic increase upon application of a quite low longitudinal magnetic field that dynamically reduces the spin relaxation. Moreover, we show that the parasitic contribution of the MCD [1,37] can be completely suppressed by setting an appropriate balance between electron and hole currents. However, the performance of the device remains limited by a dynamical factor accounting for the matching between the recombination and tunneling times: a mismatch leads to a decrease of the spin asymmetry, explaining the weak values of only a few percent reported in the literature. This fundamental limitation can be overcome by increasing the tunnel resistance, i.e., the tunnel time similarly to the conductivity mismatch problem, while optimizing an appropriate figure of merit. The present results pave the way to the development of a future generation of optoelectronic devices for the conversion of information carried by the photon helicity into an electrical signal.

This work has been supported by a public grant overseen by the Agence Nationale de Recherche (ANR) as part of the "Investissements d'Avenir" program (Labex NanoSaclay, ANR-10-LABX-0035)". I. V. R. thanks the Metchnikov program of the French Embassy in Russia, the visiting scientist program of the École Polytechnique, and the Foundation for the Advancement of Theoretical Physics and Mathematics BASIS for support. Y. L. acknowledges the support by ANR SIZMO2D (ANR-19-CE24-0005), FEOrgSpin (ANR-18-CE24-0017), and SISTER (ANR-11-IS10-0001). The ferromagnetic structure was grown at the platform TUBE-Davm funded by ERDF (EU), ANR, Region Lorraine, and Grand Nancy. B. X would acknowledge the support by the National Key R&D Program of China (2018YFB2200104). We are grateful to Xavier Marie and Igor Žutić for valuable discussions. We thank Olivier Cavani and Audrey Courpron for technical help, and Travis Wade for critical reading of the manuscript.

*Corresponding author.
henri-jean.drouhin@polytechnique.edu

[1] N. Nishizawa and H. Munekata, Lateral-type spin-photonics devices: Development and applications, Micromachines **12**, 644 (2021).

[2] R. Fiederling, M. Keim, G. Reuscher, W. Ossau, G. Schmidt, A. Waag, and L. W. Molenkamp, Injection and detection of a spin-polarized current in a light-emitting diode, Nature (London) **402**, 787 (1999).

[3] X. Jiang, R. Wang, R. M. Shelby, R. M. Macfarlane, S. R. Bank, J. S. Harris, and S. S. P. Parkin, Highly Spin-Polarized Room-Temperature Tunnel Injector for Semiconductor Spintronics Using MgO(100), Phys. Rev. Lett. **94**, 056601 (2005).

[4] S. H. Liang *et al.*, Large and robust electrical spin injection into GaAs at zero magnetic field using an ultrathin CoFeB/MgO injector, Phys. Rev. B **90**, 085310 (2014).

[5] B. Tao, P. Barate, X. Devaux, P. Renucci, J. Frougier, A. Djeffal, S. Liang, B. Xu, M. Hehn, H. Jaffrès, J.-M. George, X. Marie, S. Mangin, X. Han, Z. Wang, and Y. Lu, Atomic-scale understanding of high thermal stability of the Mo/CoFeB/MgO spin injector for spin-injection in remanence, Nanoscale **10**, 10213 (2018).

[6] I. Žutić, G. Xu, M. Lindemann, P. E. Faria Junior, J. Lee, V. Labinac, K. Stojšić, G. M. Sipahi, M. R. Hofmann, and N. C. Gerhardt, Spin-lasers: Spintronics beyond magnetoresistance, Solid State Commun. **316–317**, 113949 (2020).

[7] M. Lindemann, G. Xu, T. Pusch, R. Michalzik, M. R. Hofmann, I. Žutić, and N. C. Gerhardt, Ultrafast spin-lasers, Nature (London) **568**, 212 (2019).

[8] T. Kondo, J.-j. Hayafuj, and H. Munekata, Investigation of spin voltaic effect in a *p-n* Heterojunction, Jpn. J. Appl. Phys. **45**, L663 (2006).

[9] I. Žutić, J. Fabian, and S. Das Sarma, Spin injection through the depletion layer: A theory of spin-polarized *p-n* junctions and solar cells, Phys. Rev. B **64**, 121201(R) (2001).

[10] A. Hirohata, Y. B. Xu, C. M. Guertler, and J. A. C. Bland, Spin-dependent electron transport at the ferromagnet/semiconductor interface, J. Appl. Phys. **85**, 5804 (1999).

[11] A. F. Isakovic, D. M. Carr, J. Strand, B. D. Schultz, C. J. Palmstrøm, and P. A. Crowell, Optical pumping in ferromagnet-semiconductor heterostructures: Magneto-optics and spin transport, Phys. Rev. B **64**, 161304(R) (2001).

[12] T. Taniyama, G. Wastlbauer, A. Ionescu, M. Tselepi, and J. A. C. Bland, Spin-selective transport through Fe/AlOx/GaAs(100) interfaces under optical spin orientation, Phys. Rev. B **68**, 134430 (2003).

[13] X. Jiang, R. Wang, S. van Dijken, R. Shelby, R. Macfarlane, G. S. Solomon, J. Harris, and S. S. P. Parkin, Optical Detection of Hot-Electron Spin Injection into GaAs from a Magnetic Tunnel Transistor Source, Phys. Rev. Lett. **90**, 256603 (2003).

[14] P. Renucci, V. G. Truong, H. Jaffrès, L. Lombez, P. H. Binh, T. Amand, J. M. George, and X. Marie, Spin-polarized electroluminescence and spin-dependent photocurrent in hybrid semiconductor/ferromagnetic heterostructures: An asymmetric problem, Phys. Rev. B **82**, 195317 (2010).

[15] C. Rinaldi, M. Cantoni, D. Petti, A. Sottocorno, M. Leone, N. M. Caffrey, S. Sanvito, and R. Bertacco, Ge-based spin-photodiodes for room-temperature integrated detection of photon helicity, Adv. Mater. **24**, 3037 (2012).

[16] B. Endres, M. Ciorga, M. Schmid, M. Utz, D. Bougeard, D. Weiss, G. Bayreuther, and C. H. Back, Demonstration of the spin solar cell and spin photodiode effect, Nat. Commun. **4**, 2068 (2013).

[17] L. Zhu, W. Huang, P. Renucci, X. Marie, Y. Liu, Y. Li, Q. Wu, Y. Zhang, B. Xu, Y. Lu, and Y. Chen, Angular Dependence of the Spin Photocurrent in a Co—Fe—B/MgO/$n-i-p$ GaAs Quantum-Well Structure, Phys. Rev. Applied **8**, 064022 (2017).

[18] R. C. Roca, N. Nishizawa, K. Nishibayashi, and H. Munekata, Investigation of helicity-dependent photocurrent at room temperature from a Fe/x-AlO x /p-GaAs schottky junction with oblique surface illumination, Jpn. J. Appl. Phys. **56**, 04CN05 (2017).

[19] A. Djeffal, F. Cadiz, M. Stoffel, D. Lagarde, X. Gao, H. Jaffrès, X. Devaux, S. Migot, X. Marie, H. Rinnert, S. Mangin, J.-M. George, P. Renucci, and Y. Lu, Co-Fe-B/MgO/Ge Spin Photodiode Operating at Telecommunication Wavelength with Zero Applied Magnetic Field, Phys. Rev. Applied **10**, 044049 (2018).

[20] X. Xue, L. Zhu, W. Huang, X. Marie, P. Renucci, Y. Liu, Y. Zhang, X. Zeng, J. Wu, B. Xu, Z. Wang, Y. Chen, W. Zhang, and Y. Lu, Comparison of spin photocurrent in devices based on in-plane or out-of-plane magnetized CoFeB spin detectors, Phys. Rev. B **100**, 045417 (2019).

[21] A. E. Giba, X. Gao, M. Stoffel, X. Devaux, B. Xu, X. Marie, P. Renucci, H. Jaffrès, J.-M. George, G. Cong, Z. Wang, H. Rinnert, and Y. Lu, Spin Injection and Relaxation in p-doped (In, Ga)As/GaAs Quantum-Dot Spin Light-Emitting Diodes at Zero Magnetic Field, Phys. Rev. Applied **14**, 034017 (2020).

[22] F. Meier and B. P. Zakharchenya, *Optical Orientation* (North-Holland, Amsterdam, 1984), https://www.sciencedirect.com/bookseries/modern-problems-in-condensed-matter-sciences/vol/8/suppl/C.

[23] Y.-H. Kim, Y. Zhai, H. Lu, X. Pan, C. Xiao, E. A. Gaulding, S. P. Harvey, J. J. Berry, Z. V. Vardeny, J. M. Luther, and M. C. Beard, Chiral-induced spin selectivity enables a room-temperature spin light-emitting diode, Science **371**, 1129 (2021).

[24] C. Chen, L. Gao, W. Gao, C. Ge, X. Du, Z. Li, Y. Yang, G. Niu, and J. Tang, Circularly polarized light detection using chiral hybrid perovskite, Nat. Commun. **10**, 1927 (2019).

[25] D. Niesner, M. Hauck, S. Shrestha, I. Levchuk, G. J. Matt, A. Osvet, M. Batentschuk, C. Brabec, H. B. Weber, and T. Fauster, Structural fluctuations cause spin-split states in tetragonal $(CH_3NH_3)PbI_3$ as evidenced by the circular photogalvanic effect, Proc. Natl. Acad. Sci. U.S.A. **115**, 9509 (2018).

[26] G. Schmidt, D. Ferrand, L. W. Molenkamp, A. T. Filip, and B. J. van Wees, Fundamental obstacle for electrical spin injection from a ferromagnetic metal into a diffusive semiconductor, Phys. Rev. B **62**, R4790 (2000).

[27] S. P. Dash, S. Sharma, J. C. Le Breton, J. Peiro, H. Jaffrès, J.-M. George, A. Lemaître, and R. Jansen, Spin precession and inverted Hanle effect in a semiconductor near a finite-roughness ferromagnetic interface, Phys. Rev. B **84**, 054410 (2011).

[28] F. Cadiz, A. Djeffal, D. Lagarde, A. Balocchi, B. Tao, B. Xu, S. Liang, M. Stoffel, X. Devaux, H. Jaffrès, J.-M. George, M. Hehn, S. Mangin, H. Carrere, X. Marie, T. Amand, X. Han, Z. Wang, B. Urbaszek, Y. Lu, and P. Renucci, Electrical initialization of electron and nuclear spins in a single quantum dot at zero magnetic field, Nano Lett. **18**, 2381 (2018).

[29] See Supplemental Material at http://link.aps.org/supplemental/10.1103/PhysRevLett.128.057701 for additional information on the sample structure, magnetic characterizations and analytical derivations of the formulas used in the present Letter.

[30] M. I. Dyakonov, *Spin Physics in Semiconductors* (Springer, Berlin, 2008), https://link.springer.com/book/10.1007/978-3-540-78820-1.

[31] X. Liu, N. Tang, C. Fang, C. Wan, S. Zhang, X. Zhang, H. Guan, Y. Zhang, X. Qian, Y. Ji, W. Ge, X. Han, and B. Shen, Spin relaxation induced by interfacial effects in n-GaN/MgO/Co spin injectors, RSC Adv. **10**, 12547 (2020).

[32] P. Bruno, Dipolar magnetic surface anisotropy in ferromagnetic thin films with interfacial roughness, J. Appl. Phys. **64**, 3153 (1988).

[33] J. Moritz, F. Garcia, J. C. Toussaint, B. Dieny, and J. P. Nozières, Orange peel coupling in multilayers with perpendicular magnetic anisotropy: Application to Co/Pt-based exchange-biased spin-valves, Europhys. Lett. **65**, 123 (2004).

[34] V. L. Berkovits, A. I. Ekimov, and V. I. Safarov, Optical orientation in a system of electrons and lattice nuclei in semiconductors. Experiment, Sov. Phys. JETP **38**, 169 (1974), http://jetp.ras.ru/cgi-bin/e/index/e/38/1/p169?a=list.

[35] M. I. Dyakonov and V. I. Perel’, Optical orientation in a system of electrons and lattice nuclei in semiconductors. Theory, Sov. Phys. JETP **38**, 177 (1974), http://jetp.ras.ru/cgi-bin/e/index/e/38/1/p177?a=list.

[36] R. I. Dzhioev, K. V. Kavokin, V. L. Korenev, M. V. Lazarev, B. Y. Meltser, M. N. Stepanova, B. P. Zakharchenya, D. Gammon, and D. S. Katzer, Low-temperature spin relaxation in n-type GaAs, Phys. Rev. B **66**, 245204 (2002).

[37] S. J. Steinmuller, C. M. Gürtler, G. Wastlbauer, and J. A. C. Bland, Separation of electron spin filtering and magnetic circular dichroism effects in photoexcitation studies of hybrid ferromagnet/GaAs schottky barrier structures, Phys. Rev. B **72**, 045301 (2005).